Quantitative Spatiotemporal Analysis of Antibody Fragment Diffusion and Endocytic Consumption in Tumor Spheroids

Greg M. Thurber[1] and K. Dane Wittrup[1,2]

Departments of [1]Chemical Engineering and [2]Biological Engineering, Massachusetts Institute of Technology, Cambridge, Massachusetts

Abstract

Antibody-based cancer treatment depends upon distribution of the targeting macromolecule throughout tumor tissue, and spatial heterogeneity could significantly limit efficacy in many cases. Antibody distribution in tumor tissue is a function of drug dosage, antigen concentration, binding affinity, antigen internalization, drug extravasation from blood vessels, diffusion in the tumor extracellular matrix, and systemic clearance rates. We have isolated the effects of a subset of these variables by live-cell microscopic imaging of single-chain antibody fragments against carcinoembryonic antigen in LS174T tumor spheroids. The measured rates of scFv penetration and retention were compared with theoretical predictions based on simple scaling criteria. The theory predicts that antibody dose must be large enough to drive a sufficient diffusive flux of antibody to overcome cellular internalization, and exposure time must be long enough to allow penetration to the spheroid center. The experimental results in spheroids are quantitatively consistent with these predictions. Therefore, simple scaling criteria can be applied to accurately predict antibody and antibody fragment penetration distance in tumor tissue. [Cancer Res 2008;68(9):3334–41]

Introduction

Antibodies are being applied for specific tumor targeting of a variety of treatment modalities (Fc effector functions, signaling disruption, toxins, radiation, etc.). Despite their promise, a variety of problems have hampered antibody development for the treatment of solid tumors. Of the antibody treatments currently on the market, the majority are for leukemias and lymphomas despite the higher prevalence of solid tumors. There are a variety of reasons for this discrepancy, such as sensitivity of leukemias and lymphomas to treatment (e.g., radiation) and accessibility to secondary mediators (e.g., complement and effector cells). Inefficient transport of the antibody from the site of administration (typically the plasma after i.v. injection) to the site of action in the tumor precludes these molecules from binding and treating many cancerous cells (1). This deficiency includes both total uptake within a tumor as well as the distribution of the antibody once it reaches the diseased tissue. A variety of factors contribute to this problem. High cell and extracellular matrix density and high vascular fluid permeability paired with decreased functional lymphatics cause an increase in interstitial pressure (2). This results in negligible fluid flow (convection) within the interstitium of most solid tumors, leaving diffusion as the major method of transport (3). In contrast, convection is the dominant mode of macromolecular transport in healthy tissue (4). Poor extravasation from the lack of convection and low vascular density in tumors keep the supply of antibody low relative to other tissues. Once extravasated, additional hurdles to antibody movement through the tumor include internalization, slow diffusion, poor retention, and systemic clearance, which all keep the total antibody exposure low (5).

A clear example of poor transport comes from radioimmunotherapy studies. The mechanism of cell killing from radiation is well-understood, and given a sufficient dose of radiation, the tumor cells will be killed. However, due to slow uptake, the exposure of the tumor is not greatly increased over normal tissue (even in some xenograft systems where normal tissues completely lack antigen; ref. 6). Given that the ideal therapeutic outcome would be tumor doses large enough to kill the most resistant cancer cells while sparing the most sensitive healthy tissue (typically bone marrow), demands on uptake are fairly stringent and apparently difficult to achieve. If the cell killing mechanism cannot destroy tumor cells faster than division can replace them, the tumor will continue to grow.

Previous modeling efforts have considered the distribution of antibodies in tumor tissue. Numerical simulations of the microdistribution around vessels (7) and physiologically based pharmacokinetic models indicate that binding increases the heterogeneity of antibody distribution and uptake in tumors is slow relative to other tissues (8). By analyzing the rate determining steps in uptake and distribution, simple criteria can be derived to quantitatively describe the distribution of antibodies within tumor tissue (5). These criteria are based on independently measured variables determined previously or straightforwardly obtainable from cell culture experiments, increasing their predictive power. Without fitting any variables to tumor uptake data, these predictions are not restricted to the systems used for data fitting. The simplicity of these criteria also makes trends, trade-offs, and predictions more intuitively accessible than for many numerical simulation exercises.

A simplified model of uptake indicates that high-affinity antibodies bind much faster than they diffuse (9). Thus, antigen is saturated cell layer after layer as the antibody diffuses into a spheroid or out of a capillary (5). After the antibody has substantially cleared from the system, the antibody front seems "frozen" in position either near the capillary wall or surface of the spheroid. Likewise, if internalization of the antigen occurs at a fast enough rate, the antibody diffusing into the tumor tissue degrades before reaching deeper into the tumor, and again, the antibody front seems "frozen" in place. Theoretical models predict the existence of such a dynamic steady-state balance between antibody penetration and degradation (5, 9).

In this work, we examine the diffusion, binding, and distribution of antibody single chain variable fragments (scFv) against carcinoembryonic antigen (CEA) in tumor spheroids. The behavior of full IgG antibodies compared with scFvs is quantitatively

Note: Supplementary data for this article are available at Cancer Research Online (http://cancerres.aacrjournals.org/).

Requests for reprints: K. Dane Wittrup, Department of Biological Engineering, Massachusetts Institute of Technology, Cambridge, MA 02139. Phone: 617-253-4578; E-mail: Wittrup@mit.edu.

doi:10.1158/0008-5472.CAN-07-3018

different (due to differences in the diffusion coefficient, void fraction, and bivalent binding), and these differences are captured in the theoretical model. Qualitatively, these molecules transport in a similar fashion, allowing model predictions for antibodies, antibody fragments, and other binding macromolecules. Model variables for scFvs were measured independently in separate experiments and used to predict the distribution in tumor spheroids. Penetration experiments were carried out in LS174T colon cancer tumor spheroids, compared with model predictions, and found to be in excellent quantitative agreement. This provides experimental validation for the previously described tumor penetration criteria, which will enable simplified and more general consideration of the process of antibody and antibody fragment distribution in tumor tissue.

Materials and Methods

Variables for the model were measured independently to make accurate predictions of spheroid penetration. All experiments were carried out at 37°C using a tissue culture incubator or heated microscope stage unless otherwise indicated. The number of antigens per cell was measured using an Alexa 488–labeled (Invitrogen) anti-CEA antibody M111147 (Fitzgerald Industries). LS174T cells (American Type Culture Collection) were labeled along with Quantum Simply Cellular beads (Bangs Laboratories) according to the manufacturer's instructions. Flow cytometry was done on a Coulter EPICS XL flow cytometer. Cell density was determined by counting Hoechst33342-stained nuclei (Invitrogen) in a known volume of tissue under the microscope. Combined with antigens per cell, this gives the overall concentration of antigen in the tumor (Ag). To assess void fraction (ε), an irrelevant nonbinding scFv (4M5.3 that binds fluorescein) was fluorescently labeled and allowed to diffuse into a spheroid. Using a two-photon microscope, the fluorescent intensity inside the spheroid was compared with the fluorescent intensity outside the spheroid. Assuming the accessible volume outside the spheroid is 100%, the effective void fraction inside the spheroid could be found by a simple ratio. The scFvs were secreted from yeast and purified by metal affinity and size exclusion chromatography as described previously (10). Reducing and nonreducing SDS-PAGE showed a single, monovalent band of the expected molecular weight. Competitive binding to the surface of LS174T cells was used to verify the affinity and specificity of binding to CEA. After fluorophore conjugation and dialysis, TLC was used to verify the absence of free fluorophore (data not shown). The scFv concentrations were measured by absorption 280 ($[Ab]_{surf}$). The diffusion coefficient (D) was measured by diffusion of a nonbinding irrelevant scFv. Details can be found in the Supplementary Data, but briefly, fluorescent scFv was added to a spheroid at time zero and a series of confocal images were taken over time. The fluorescence intensity within the spheroid was averaged over the radius and adjusted for the total volumetric fluorescence intensity. Because diffusion is the only method of transport in these spheroids, the signal was normalized to long times and the diffusion coefficient was fit according to the series solution of diffusion in a sphere assuming Fick's law (11). This method not only accounts for slower diffusion due to extracellular matrix but also the constricted and tortuous path between cells. The internalization rate for CEA binders (k_e) was calculated in a separate article,[3] and the radius of the spheroids (R) was measured from the microscopic image.

Spheroids were grown by the hanging drop method (12) using microwell trays (Nunc). Briefly, 500 cells per well of LS174T cells were incubated upside down at 37°C and 5% CO_2 for 2 d to allow cohesion between cells. They were then transferred to Lab-Tek dishes (Nunc) for 2 d to allow attachment to the cover glass. Fluorescent scFv was added to the wells for a given time before or during imaging. Details of the spheroid data analysis can be found in the Supplementary Data. Briefly, scFvs (sm3E with a K_d of 30 pmol/L; shMFE, K_d = 8 nmol/L; ref. 10) were incubated with spheroids for a given period of time. Images were taken on a Zeiss confocal microscope (Zeiss) or Zeiss microscope with Spectra-Physics Ti-Sa laser for the two-photon imaging. The confocal and two-photon imaging allowed all images (except Fig. 5) to be taken in the presence of antibody in the bulk solution, yielding uninterrupted sequential images. The data from high-affinity antibody fragments were analyzed by despeckling the image and creating a binary threshold just above background and autofluorescence. The purpose was to select only those pixels where binding increased the fluorescence above background. A series of dilations (and equal number of erosions) was used to fill in small holes in the ring-shaped masks. The outer and inner areas of the ring structure were measured (yielding the total spheroid and untargeted core areas), and the spheroid radius and radius of scFv penetration were then calculated assuming sphericity (area averaged). Green fluorescent beads (Duke Scientific) were added to the wells to serve as internal controls. Although they had no direct effect on analysis of the data, consistent fluorescence intensity of these beads verified exposure conditions were constant across all experiments. All image analysis was done in ImageJ (NIH).

For the IHC images, spheroids were grown in a similar manner, except they were not allowed to adhere to the cover glass. Antibody fragment incubations were done in the hanging drop. The spheroids were then fixed and processed in MIT's Center for Cancer Research Histology facility. Details for labeling can be found in the Supplementary Data, but briefly, the slides were deparafinized, boiled in citric acid, serum blocked, and labeled with a noncompeting fluorescent antibody to mark antigen. Images were taken on a Deltavision deconvolution fluorescence microscope (Applied Precision).

Results

Diffusion and binding of fluorescently tagged scFv molecules in tumor spheroids was monitored using confocal or multiphoton fluorescence microscopy, and the distance of penetration of these molecules was then compared with theoretical predictions. The scaling criteria used for these predictions consist of two moduli, which are ratios of variables that capture fundamental rates (clearance, diffusion, internalization, etc.) that determine antibody and antibody fragment distribution. To make accurate predictions of antibody penetration with the clearance modulus and Thiele modulus criteria (5), all the pertinent variables were measured independently in these LS174T spheroids. The individual variables, as outlined in Materials and Methods, were determined experimentally and are presented in Fig. 1. Cell density is in line with previous estimates in other systems (13, 14), although it may be slightly higher in these spheroids than in solid tumors due to high viability and lack of other cell types. Antigen density is also in agreement with reported values (15), although variability on individual cells is high. The void fraction is slightly lower than previous estimates for scFv (16), likely due to the high cell density. The diffusion coefficient is lower than previously published values (9), and this value is averaged over the entire spheroid, which incorporates the effects of extracellular matrix, tortuosity, and constriction between cells.

Live-cell imaging of fluorescently labeled scFvs allowed the collection of dynamic diffusion and binding data. These spheroids are highly scattering, so even two-photon microscopy was not able to image in the center of the spheroids without geometric artifacts and low signal to noise. To circumvent this problem, the spheroids were first allowed to attach to coverslips. After sufficient time for attachment, diffusion of scFvs between the coverslip and the spheroid is negligible, as seen previously (17). This results in a "physical slice" (the coverslip) through the spheroid (Fig. 1). The optical slicing ability of the two-photon microscope was used to image deeper into the spheroid to verify that scFv was not diffusing more rapidly near the coverslip.

[3] M.M. Schmidt, G.M. Thurber, and K.D. Wittrup. Kinetics of Anti-Carcinoembryonic Antigen (CEA) Antibody Internalization: Effects of Affinity Bivalency, and Stability. Cancer Immun Immunother, submitted for publication.

Parameter	Value	Abs Error
Cell density	7.23 x 10^8 cell/mL	+/- 1.87 x 10^8
Ag per cell	3.88 x 10^5 Ag/cell	+/- 4.7 x 10^3
Antigen density	4.68 x 10^{-7} mol/L	+/- 1.27 x 10^{-7}
Epsilon	0.1537	+/-0.011
Diffusion coefficient	33.1 $\mu m^2/s$	+/-20.7
k_e	1.23 x 10^{-5} s^{-1}	+/- 3.06 x 10^{-6}

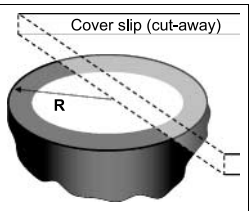

Figure 1. Experimental imaging setup and measured variable values. Spheroids were allowed to attach to the cover glass and form a hemisphere shape. All the variable values were measured separately to give an independent theoretical prediction for scFv distribution.

Antibody penetration into tumor tissue *in vivo* is predicted to be a function of exposure time and concentration, or the area under the curve (AUC; refs. 5, 9). In this *in vitro* system, there is no clearance of the antibody fragment, so the concentration is constant over time. The AUC in this spheroid system is just the concentration outside the spheroid multiplied by the incubation time. In other words, spheroids need to be incubated for a sufficient period of time for the antibody to reach the center, and this time is a function of spheroid size, diffusion coefficient, antigen, and antibody concentrations. In the absence of antibody metabolism, this penetration time is predicted to be (9):

$$t_{sat} = \frac{R^2([Ag]/\varepsilon)}{6D[Ab]_{surf}}$$

Figure 2 shows experimental images of dynamic penetration of scFv into a spheroid. Using 100 nmol/L concentration of sm3E, the antibody fragment saturated the spheroid after 95 minutes of incubation (predicted time from the above formula is 57 minutes). This is in contrast to a nonbinding scFv (4M5.3) that reaches 90% of total signal in 3 minutes due to lack of binding (Supplementary Data) or lower concentrations of sm3E that do not penetrate after 48 hours (and are theoretically predicted to never reach the center because endocytic consumption exceeds diffusive flux). With such rapid penetration, antibody internalization (~ 15-hour half-life) has a negligible effect on the saturation time. Although saturation is predicted to occur faster than measured in the experiment, much of this may be due to nonspecific sticking of the antibody fragment. At concentrations above ~ 20 nmol/L, scFv begins to adhere to the surface of cells (data not shown), requiring more scFv to diffuse into the spheroid to specifically bind the antigen.

Looking at the above saturation time predicted by the clearance modulus, low doses of sm3E will reach every cell given sufficient exposure time. However, the Thiele modulus predicts that there is a threshold dose required to overcome internalization and metabolism of surface-bound antibody fragment to saturate all cells at steady state. Spheroids were incubated at low doses of sm3E for long periods of time (48 hours), and the radius of antigen saturation was measured. The experimental threshold dose required for saturation closely matches the theoretical prediction (Fig. 3, *left*). In all cases, the scFv was in excess at least 10-fold over antigen to avoid depletion in the bulk solution.

To further show that the lack of penetration is due to the slow internalization and degradation of scFv bound to antigen, spheroids were incubated at room temperature for 48 hours at equivalent concentrations. Internalization is significantly diminished at room temperature (data not shown), and antibody is able to reach the center (Fig. 3, *right*). In the absence of internalization, a reduction in temperature would actually be expected to *decrease* the penetration distance by somewhat reducing the diffusion coefficient (18).

Low affinity antibody fragments are predicted to have more homogenous distribution in tumor tissue (19), and this has been verified experimentally (20). To examine this effect in the spheroid system, a lower affinity variant of the sm3E scFv was used. This scFv, shMFE, has a dissociation constant of 8 nmol/L versus the 30 pmol/L dissociation constant of sm3E. There are only two amino acid changes between these scFvs, so affinity is the primary difference (10). As shown in Fig. 4, the "low" affinity shMFE has a much more homogenous distribution in the spheroid compared with the bottom panel, which shows the heterogeneous distribution of the high-affinity scFv. However, also note that the concentrations for shMFE are much higher than for sm3E to bind a significant fraction of antigen. At the highest shMFE concentration (100 nmol/L), the free scFv in the bulk is approaching the antigen concentration in the spheroid (500 nmol/L). This distribution is in agreement with numerical simulations of antibody and antibody fragment penetration (Fig. 4, *right*).

Although numerical simulations are useful, scaling analyses can also be used to determine the affinity necessary for a more homogenous distribution. If $[Ab]_{surf}$ is replaced with K_d in the clearance or Thiele modulus terms, this scaling variable determines whether antibody will reach a given radius (21). Note that for low affinity antibody fragments, this does not mean antigen is saturated to this radius. It only means that by repetitive binding, dissociation, and diffusion, some scFv was able to reach the given radius.

$$\phi^2 = \frac{k_e R^2([Ag]/\varepsilon)}{D(K_d + [Ab]_{surf})} \qquad t_{center} = \frac{R^2([Ag]/\varepsilon)}{D(K_d + [Ab]_{surf})}$$

As affinity increases from that of shMFE to sm3E, the model predicts that the distribution will become increasingly heterogeneous as more scFv is bound at the higher affinities.

Due to the fact that a higher proportion of low affinity scFvs are not bound, they may not be adequately retained after the free antibody fragment is removed from the surface of the spheroid. The persistence of scFv in the spheroid after free scFv was removed from the bulk was directly tested in the spheroids. Spheroids were incubated with 20 nmol/L sm3E or shMFE for 2.5 hours to quickly bind antigen. The dose was kept low to minimize nonspecific sticking, and the time was short to minimize internalization during the binding phase, although this results in incomplete saturation. After this brief incubation, the medium was exchanged to remove free antibody fragment, and the spheroids were incubated for 48 hours. Figure 5 shows the images after this "wash out" period. The high-affinity sm3E has a much stronger signal after 48 hours. The

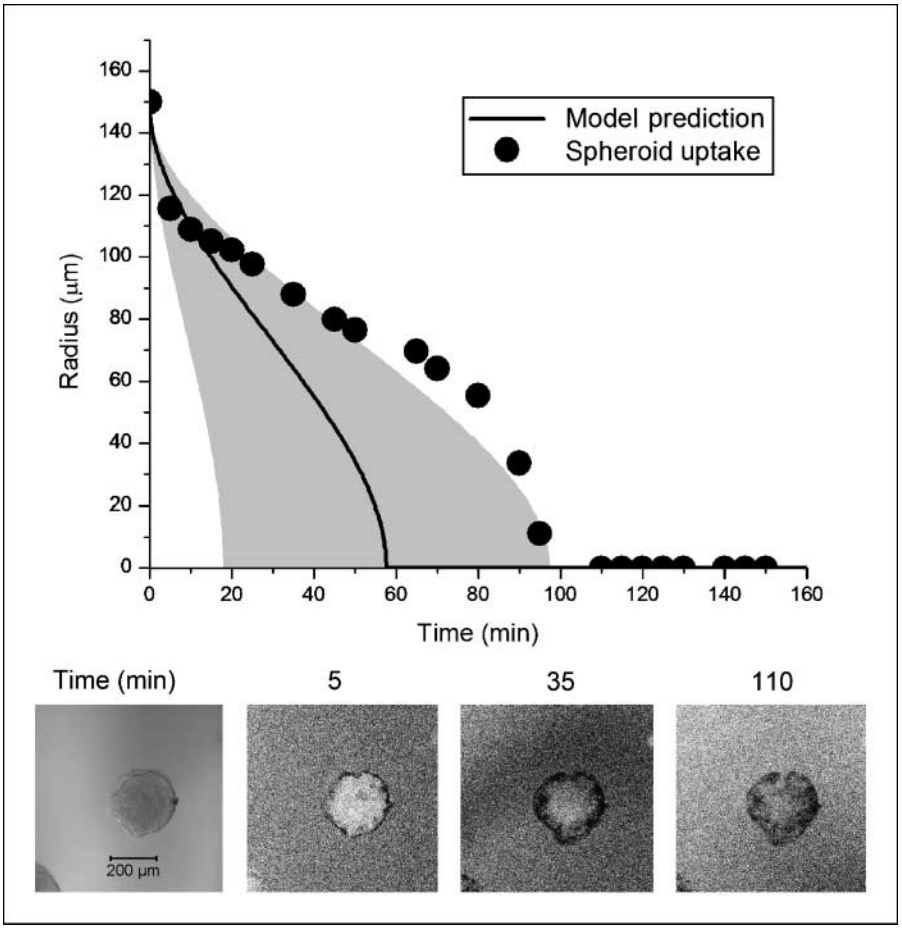

Figure 2. Live sm3E diffusion with binding in spheroids. *Top,* radius of the moving scFv front as a function of time (•). *Black line,* theoretical prediction; *gray shaded area,* ±SD from the theoretical prediction due to error in the experimentally measured variables. *Bottom,* differential interference contrast (*DIC*) image and three fluorescence images at various time points. The high background is due to the 100 nmol/L fluorescent scFv present in the bulk solution. *Scale bar,* 200 μm.

Alexa 488 dye used in these studies remains inside the cells for an extended period of time after internalization (data not shown). Therefore, much of the signal that is seen may be from internalized antibody for both sm3E and shMFE. Numerical simulations provide further insights into this experiment. The high-affinity sm3E remains bound such that very little diffuses out of the spheroid, and the total signal is high. After 2 days, the antigen turn-over (15-hour half-life) has internalized a significant fraction of antibody fragment, but 15% still remains on the surface. The results are much different for the low affinity scFv. The rapid release and low

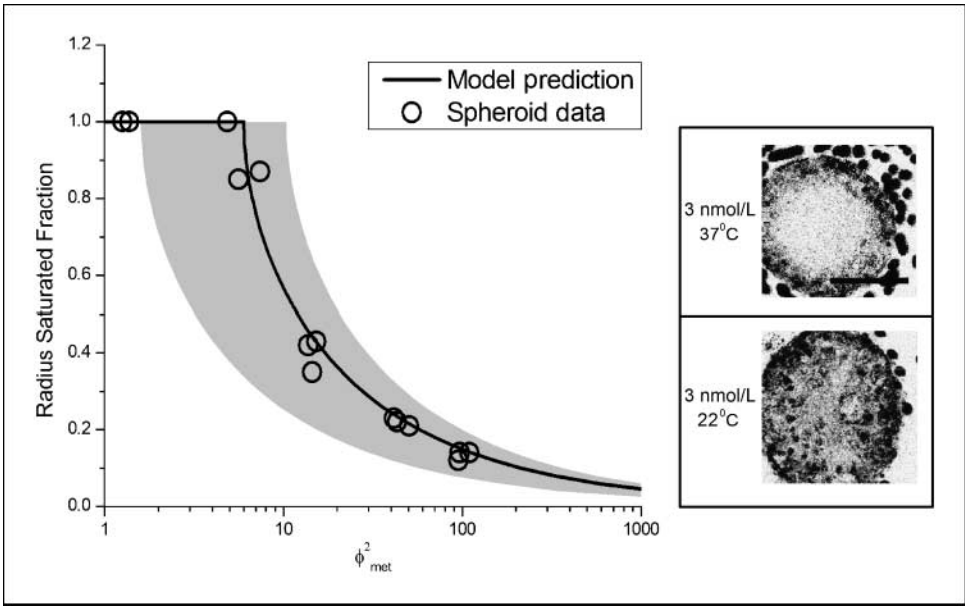

Figure 3. Steady-state spheroid depth of saturation. *Left,* the saturated fraction of the radius $[(R_{tumor} - r_{antibody\ front})/R_{tumor}]$ is plotted as a function of the Thiele modulus. ○, measured values for individual spheroids; *black line,* theoretical prediction. *Gray shaded area,* ±SD from the theory due to uncertainty in the experimentally measured variables. Complete saturation occurs at a φ^2 of 6 because the geometric shape factor of 6 (for spheres) that arises in the exact solution is not included in the Thiele modulus. *Right,* images of two spheroids incubated at different temperatures are shown. Antibody fragment reaches the center at room temperature when internalization is reduced. *Dark circles surrounding the spheroids,* green fluorescent beads serving as internal controls. *Scale bar,* 200 μm.

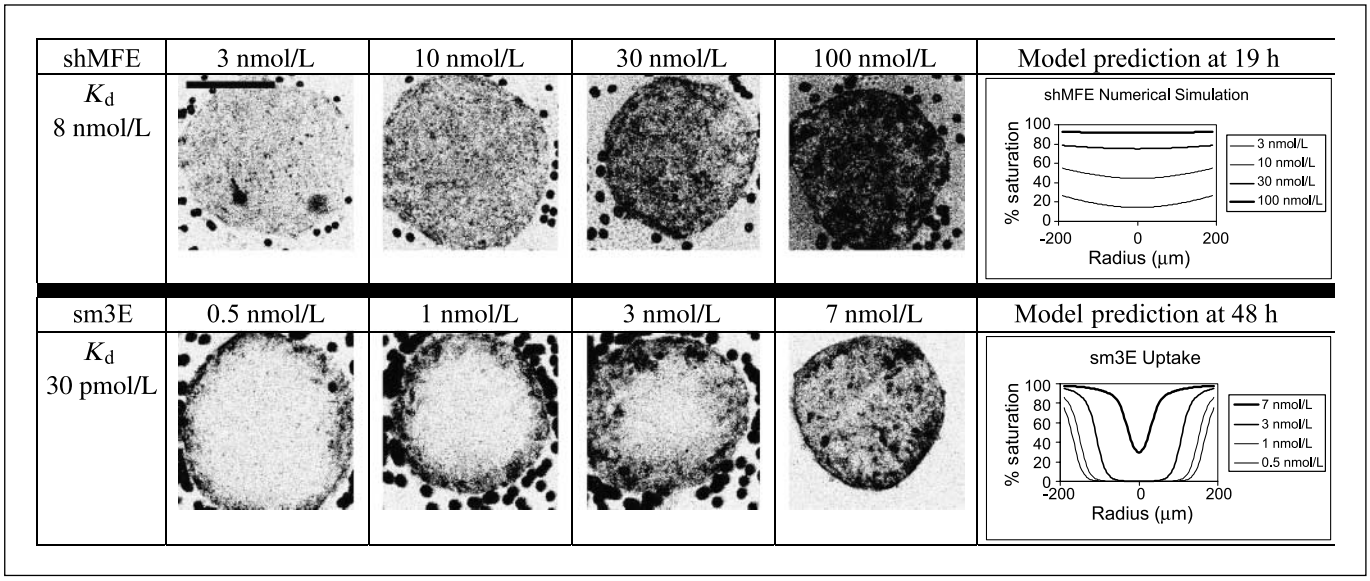

Figure 4. Low-affinity versus high-affinity distribution. *Top,* images of spheroids exposed to various concentrations of shMFE for 19 h are shown alongside the model predictions from numerical simulations (*right*). The high background is caused by fluorescent scFv in the bulk solution. *Bottom,* spheroids were incubated with different concentrations of sm3E for 48 h. Notice the concentrations are much lower for the high-affinity scFv. Numerical simulation predictions are shown on the right. All images are adjusted to the same level of contrast. *Scale bar,* 200 μm.

fraction of bound scFv allows more homogenous penetration, but it also allows the antibody fragment to diffuse out of the spheroid. After 48 hours, much of the total signal is gone. The signal that does remain has all been internalized, and <0.5% of the antigen is predicted to be bound on the surface.

To validate the microscope-imaging techniques used, spheroids were grown continually in a hanging drop without attachment to plates. They were incubated with sm3E, fixed, and analyzed by immunohistochemistry (IHC). In this setup, antigen could be labeled independently using a noncompeting IgG in addition to the fluorescent scFv to look at colocalization. Figure 6 (*top*) shows sm3E, antigen, and merged images at three different concentrations. Looking at the scFv fluorescence, the two highest concentrations have a φ^2 of <6 and are predicted to be saturated, in agreement with the images. The lowest concentration has peripheral fluorescence indicative of the lack of penetration to the center of the spheroid. The heterogeneity of antigen on individual cells seen in flow cytometry is clearly apparent in the antigen density.

To quantitatively examine colocalization between antibody fragment and antigen, dot plots were created to evaluate the Pearson correlation coefficient. In this way, absolute intensity of either channel (microscope settings, differences in tags, etc.) does not influence the results. A major increase in the Pearson correlation coefficient occurs once the spheroid is saturated. Some correlation is expected

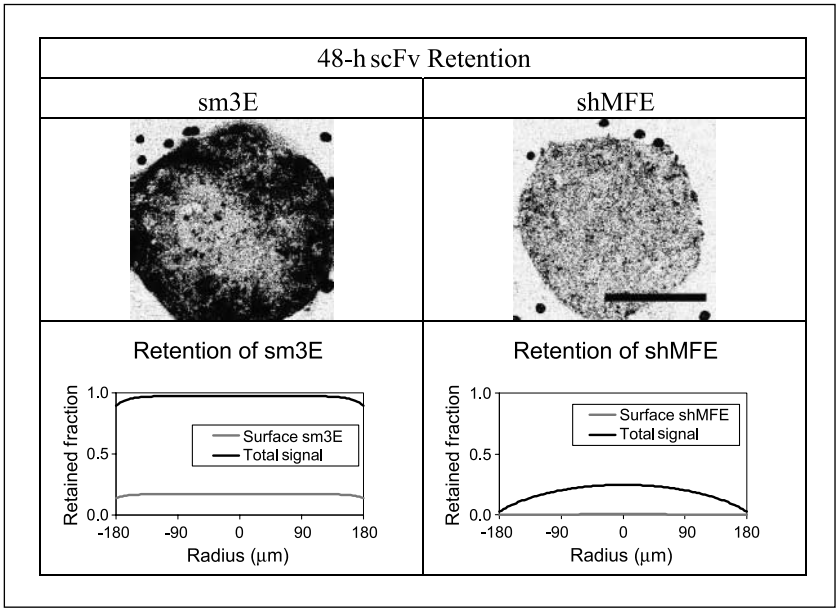

Figure 5. Retention of antibody fragment. Spheroids were incubated at 20 nmol/L concentration for 2.5 h, free scFv was removed, and they were incubated for 48 h in plain medium. *Top,* images were taken of two spheroids after the 48-h "washout" period. *Bottom,* results of a numerical simulation where the spheroids were initially at equilibrium with 20 nmol/L scFv then moved to scFv free medium for 48 h. *Scale bar,* 200 μm.

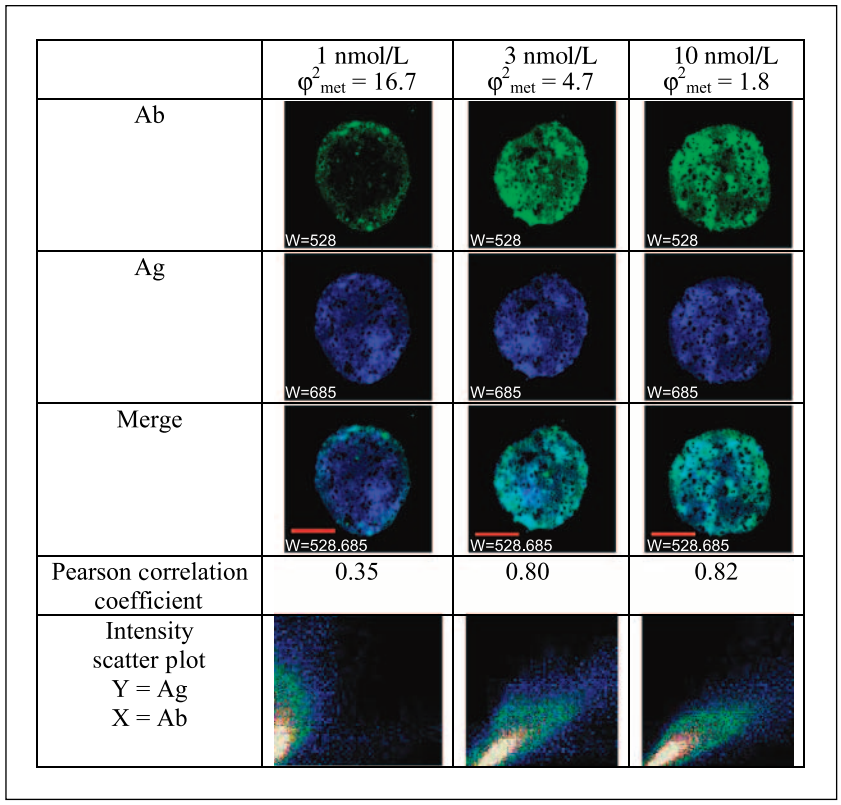

Figure 6. IHC analysis of antibody fragment penetration. *Top,* spheroids were incubated in suspension with three different concentrations of green fluorescent sm3E scFv for 48 h. The spheroids were then processed for IHC and labeled with a noncompeting anti-CEA antibody (*blue fluorescence*). The two highest concentrations have a φ^2 of <6 and are predicted to be saturated. *Bottom,* Pearson correlation coefficients were calculated for the fluorescence intensity of sm3E and antigen. Pixels with no fluorescence in either channel (background) were excluded from the analysis. Scatter plots of the fluorescent pixels are shown for all three images. *Scale bar,* 100 μm.

for the unsaturated spheroid, as there should be colocalization near the surface in the region where scFv is able to penetrate.

Discussion

The tumor spheroid model system for measuring scFv penetration provides valuable insights into key aspects of antibody tumor targeting. Antibody distribution is dependent on a variety of variables, and penetration to the center of a spheroid is not simply a binary result. The dose, antigen density, spheroid size, incubation time, and all the other variables present in the clearance and Thiele moduli affect the results. The spheroids used here most closely resemble prevascular micrometastases in normal tissue. Other physiologic barriers, such as lowered concentrations in normal tissue and inefficient extravasation across tumor capillaries, are not reproduced in the spheroid model system. Therefore the *in vitro* results are not intended to directly mimic the *in vivo* results. Nevertheless, the fundamental processes of diffusion, binding, and endocytosis that determine distribution in spheroids are expected to closely replicate those acting *in vivo*.

The distribution of scFvs in these spheroids lacks a major barrier to penetration in solid tumors, namely the capillary wall. Due to elevated interstitial pressure, convection in the tumor is negligible, and the dominate mode of transport is diffusion (3), similar to the spheroids. Therefore, although the supply of antibodies is severely limited compared with these spheroids (and therefore the effective concentrations are very low), the distribution is expected to follow the same principles. Poor extravasation of macromolecules in tumors (22) results in concentrations outside the tumor capillary that can be 100- to 1,000-fold below that found in the plasma (21). The modeling results can then be modified to account for these additional complications present in vascularized tumors *in vivo*. Because the transport barriers in the spheroid system also exist *in vivo*, it is a necessary condition that a spheroid be saturated for the corresponding tumor to be saturated. Spheroid saturation is not sufficient to predict *in vivo* saturation because additional barriers exist (e.g., capillary extravasation and systemic clearance.) Modeling for the case of solid tumors compared with spheroids and metastases has been carried out previously and shown to agree with published data (5).

These experiments have shown that two simple model scaling criteria can predict the distribution of antibody fragments in spheroids. The clearance modulus, which predicts the exposure time required to saturate spheroids, and the Thiele modulus, which predicts the concentration required to overcome internalization to reach the center of a spheroid, are criteria that quantitatively capture the major determinants in antibody distribution.

Experiments with high-affinity scFvs show steep gradients as the "core" of unbound antigen "shrinks" when antibody binds the outer layers of cells. These high-affinity antibodies bind at saturating concentrations "from the outside in" (Fig. 4, *bottom*). Most IgG molecules travel through tumor tissue in this "shrinking core" fashion (saturating cell layer after cell layer) due to their rapid binding to free antigen, slow diffusion coefficients (9), and slow dissociation caused by multivalent interactions. They are often internalized before they have a chance to dissociate and diffuse farther into the tissue (23), resulting in shrinking core penetration with effectively irreversible binding. However, with newer protein engineering techniques (scFvs, Fabs, single domain antibodies, and alternative protein scaffolds), these new proteins, which are often smaller and monovalent, can exhibit "nonshrinking core" transport in tumor tissue.

Lower affinity scFvs display a more diffuse gradient, yielding more homogenous labeling of the spheroids with lower amounts of

bound antibody; they bind antigen at subsaturating concentrations "from the bottom up" (Fig. 4, *top*). If a significant fraction of antigen must be bound for the desired effect, however, much higher concentrations have to be used with the lower affinity fragments. As mentioned previously, antibody and antibody fragment concentrations in solid tumors are often very low *in vivo*. The rapid dissociation and high fraction of unbound scFv allows the lower affinity monovalent scFv to penetrate more homogenously (21). Increasing the valency would hinder complete dissociation and result in distributions similar to higher affinity binders. Unfortunately, it is the same ability to rapidly dissociate that allows scFv to diffuse back out of the tissue once the surrounding concentration has dropped.

The poor retention of lower affinity binders has implications for both imaging and pretargeting therapies. As systemic antibody is cleared from the circulation, the total signal of low-affinity antibodies will be reduced in the tumor tissue. Even if a residualizing radioisotope is used for imaging, much of this is lost due to diffusion out of the tissue before it can be internalized during the waiting period while clearance is reducing background levels. For pretargeting techniques, a waiting period is again required for normal tissue levels to drop. The surface concentration is the variable of interest because this is the only antibody accessible to secondary agents. In the retention experiment, diffusion out of the spheroid occurred much more rapidly for the low affinity scFv, resulting in higher surface concentrations for the sm3E antibody than shMFE.

Although antibody fragments rapidly diffuse in and out of spheroids, similar to a micrometastasis, the retention in solid tumors is predicted to be very different. Because the capillary wall is a significant barrier to extravasation, once the antibody has reached the tumor tissue, it is very slow to *intravasate* back into the blood. Thus, for large molecules, this enhanced permeability and retention ("EPR") effect occurs relatively independent of affinity. For smaller molecules with higher permeabilities, binding is predicted to be more important in preventing loss from the tumor due to a lower EPR effect.

Antigen labeling in the IHC experiment shows extensive CEA heterogeneity in the spheroids, as was seen on a per-cell basis in the flow cytometry experiments, and this is an important point for therapy. Looking at the merged images, the lowest concentration spheroid clearly has antigen in the center that has not been reached by sm3E. At the highest concentration, virtually every area of high antigen concentration has correspondingly high scFv concentrations, indicative of saturation. The middle concentration is more interesting. With this size spheroid, a 3 nmol/L concentration of scFv is predicted to penetrate to the center, and there is sm3E in the center as seen in the green channel. However, there is also a region in the bottom left side with very high antigen concentration that is not completely saturated by scFv. The local increase in antigen concentration (and possibly decrease in void fraction, diffusion coefficient, etc.) has apparently prevented saturation of this region. The live-cell imaging experiments would not have picked up on the high local antigen density because they only analyze the antibody fragment fluorescence signal. These IHC experiments better capture the local heterogeneities found in solid tumors and metastases. In the live-cell experiments, however, the relationship between dose and penetration distance is more clearly established despite the complicating factor of antigen heterogeneity. This antigen heterogeneity can result in antibody heterogeneity even after full antigen saturation.

A small number of fundamental processes dictate the distribution of antibodies and antibody fragments in tumor tissue, and the scaling criteria (Thiele and clearance moduli) capture these rates to better understand and predict penetration. The moduli simply relate the supply and demand of free antibody. As a bolus dose clears the plasma and normal tissues, the supply of antibody entering the tumor tissue continually shrinks, and the demand for antibody remains high as more layers of cells are bound. The clearance modulus captures this ratio and predicts the penetration distance before clearance. Similarly, even with a steady supply entering from the circulation, demand for antibody to replace molecules that were internalized or degraded may immobilize all the free antibody before it can reach every cell. This is in effect the distance that the Thiele modulus predicts.

The implications of these experiments and scaling criteria lend insight into optimizing antibody and antibody fragment imaging and therapy experiments. To target all cells with a high-affinity binder, the dose must exceed the limitations posed by clearance and internalization as given in the scaling criteria. Decreasing the clearance rate far below the antigen turn-over rate will not increase penetration into the tissue, as antibody metabolism becomes rate limiting. Lower affinity binders result in a more homogenous distribution when the K_d is large enough to reduce the scaling moduli below one. Unfortunately, the total amount entering the tumor is still small, and the fraction that is bound is even less. For prevascular metastases and proteins with high permeability, retention of these antibodies will also be poor. For imaging experiments, penetration of antibodies and fragments (and the associated signal) is directly proportional to the AUC. Increasing clearance rates reduces background noise, but it also decreases signal. A more optimal plasma profile would have an extended period of high concentration for tumor uptake followed by rapid clearance, advocating the use of clearing agents. A similar strategy would benefit pretargeting methods.

Understanding the major determinants for antibody and antibody fragment uptake, distribution, and retention in tumors and micrometastases can point to ways of improving and optimizing therapies. The requirements of bound antibody, total antibody uptake, and retention required for successful imaging and therapeutic modalities can be compared with the actual values attainable as predicted by the model based on all the relevant variables: dose, clearance, internalization, extravasation, diffusion, antigen density, and tumor vascular density. The choice of antigen target, antibody fragment size, and other protein engineering decisions can be made rationally to optimize the desired therapeutic or imaging result. Improvements in protein engineering, imaging sensitivity and resolution, toxin conjugates, Fc effector functions, signal blockade, and other areas relevant to antibody targeting will further push developments in antibody-based therapies for the diagnosis and treatment of cancer.

Acknowledgments

Received 8/6/2007; revised 12/28/2007; accepted 3/3/2008.

Grant Support: CA101830 and CA96504, and a Ludwig Fellowship (G.M. Thurber).

The costs of publication of this article were defrayed in part by the payment of page charges. This article must therefore be hereby marked *advertisement* in accordance with 18 U.S.C. Section 1734 solely to indicate this fact.

We thank the Whitehead Institute for allowing us to measure free diffusion coefficients using the W.M. Keck Foundation Biological Imaging Facility, the CCR Histology laboratory for assisting with fixing spheroids for IHC, and Hyuk-Sang Kwon and Peter So for their help and expertise with two-photon microscopy.

References

1. Jain RK. Transport of molecules, particles, and cells in solid tumors. Annu Rev Biomed Eng 1999;01:241–63.
2. Baxter L, Jain RK. Transport of fluid and macromolecules in tumors 1. Role of interstitial pressure and convection. Microvasc Res 1989;37:77–104.
3. Pluen A, Boucher Y, Ramanujan S, et al. Role of tumor-host interactions in interstitial diffusion of macromolecules: cranial vs. subcutaneous tumors. Proc Natl Acad Sci U S A 2001;98:4628–33.
4. Rippe B, Haraldsson B. Fluid and protein fluxes across small and large pores in the microvasculature. application of two-pore equations. Acta Physiol Scand 1987;131:411–28.
5. Thurber GM, Zajic SC, Wittrup KD. Theoretic criteria for antibody penetration into solid tumors and micrometastases. J Nucl Med 2007;48:995–9.
6. Goldenberg DM, Sharkey RM, Paganelli G, Barbet J, Chatal JF. Antibody pretargeting advances cancer radioimmunodetection and radioimmunotherapy. J Clin Oncol 2006;24:823–34.
7. Fujimori K, Covell D, Fletcher J, Weinstein J. Modeling analysis of the global and microscopic distribution of immunoglobulin G, F(ab')2, and Fab in Tumors. Cancer Res 1989;49:5656–63.
8. Baxter L, Zhu H, Mackensen D, Jain RK. Physiologically based pharmacokinetic model for specific and nonspecific monoclonal antibodies and fragments in normal tissues and human tumor xenografts in nude mice. Cancer Res 1994;54:1517–28.
9. Graff CP, Wittrup KD. Theoretical analysis of antibody targeting of tumor spheroids: importance of dosage for penetration, and affinity for retention. Cancer Res 2003;63:1288–96.
10. Graff C, Chester K, Begent R, Wittrup KD. Directed evolution of an anti-carcinoembryonic antigen scFv with a four-day monovalent dissociation half-time at 37°C. Protein Eng Des Sel 2004;17:293–304.
11. Crank J. The Mathematics of Diffusion. 2nd ed. Oxford: Clarendon Press; 1975.
12. Kelm J, Timmins N, Brown C, Fussenegger M, Nielsen L. Method for generation of homogenous multicellular tumor spheroids applicable to a wide variety of cell types. Biotechnol Bioeng 2003;83:173–80.
13. Ballangrud AM, Yang WH, Charlton DE, et al. Response of LNCaP spheroids after treatment with an α-particle emitter (Bi-213)-labeled anti-prostate_specific membrane antigen antibody (J591). Cancer Res 2001;61:2008–14.
14. Lyng H, Haraldseth O, Rofstad EK. Measurement of cell density and necrotic fraction in human melanoma xenografts by diffusion weighted magnetic resonance imaging. Magn Reson Med 2000;43:828–36.
15. Berk DA, Yuan F, Leunig M, Jain RK. Direct *in vivo* measurement of targeted binding in a human tumor xenograft. Proc Natl Acad Sci U S A 1997;94:1785–90.
16. Krol A, Nagaraj S, Dewhirst M, Yuan F. Available volume fraction of macromolecules in tumor tissues. FASEB J 2000;14:A167–A.
17. Myrdal S, Foster M. Time-resolved confocal analysis of antibody penetration into living, solid tumor spheroids. Scanning 1994;16:155–67.
18. Brown EB, Boucher Y, Nasser S, Jain RK. Measurement of macromolecular diffusion coefficients in human tumors. Microvasc Res 2004;67:231–6.
19. Fujimori K, Covell DG, Fletcher JE, Weinstein JN. A modeling analysis of monoclonal antibody percolation through tumors: a binding-site barrier. J Nucl Med 1990;31:1191–8.
20. Adams G, Schier R, McCall A, et al. High affinity restricts the localization and tumor penetration of single-chain Fv antibody molecules. Cancer Res 2001;61:4750–5.
21. Thurber G, Schmidt M, Wittrup KD. Factors determining antibody distribution in tumors. Trends Pharmacol Sci 2008;29:57–61.
22. Yuan F, Dellian M, Fukumura D, et al. Vascular permeability in a human tumor xenograft: molecular size dependence and cutoff size. Cancer Res 1995;55:3752–6.
23. Mattes MJ, Griffiths G, Diril H, Goldenberg D, Ong G, Shih L. Processing of antibody-radioisotope conjugates after binding to the surface of tumor cells. Cancer 1994;73:787–93.